Article

Modeling Solar Cells Operating at Waste Light †

Krzysztof Górecki *[iD], Jacek Dąbrowski [iD] and Ewa Krac [iD]

Department of Marine Electronics, Gdynia Maritime University, Morska 83, 81-225 Gdynia, Poland;
j.dabrowski@we.umg.edu.pl (J.D.); e.krac@we.umg.edu.pl (E.K.)
* Correspondence: k.gorecki@we.umg.edu.pl
† This paper is an extended version of our paper published in Proceedings of the 2019 IEEE 13th International
Conference on Compatibility, Power Electronics and Power Engineering (CPE-POWERENG), Sonderborg,
Denmark, 23–25 April 2019; pp. 1–5, doi: 10.1109/CPE.2019.8862389.

Abstract: The article concerns the investigations of solar cells irradiated by waste light. The measurement method and instruments used are presented. Using this method, the spectra of the light emitted by different light sources are presented and the results of measurements of sensitivity characteristics of the selected solar cell are shown. On the basis of the obtained results of the measurements, a new model of a solar cell dedicated for SPICE is formulated. In this model, an influence of spectrum characteristics of the modeled solar cell on its photocurrent is taken into account. The correctness of this model is verified experimentally for all the considered lighting sources. It is proved that photocurrent is the highest for irradiation using a classical bulb, whereas it is the lowest for a fluorescent lamp.

Keywords: light sources; measurements; modeling; power generation; solar cells; waste light

1. Introduction

Solar cells are basic components of photovoltaic installations, which are ecological sources of electrical energy [1–7]. These cells produce electrical energy using light radiation irradiating their surface. In many papers [2,8], photovoltaic systems of different peak values of the produced electrical power—from hundreds of watts to hundreds of megawatts—are described. Such systems account for an increasing part of electroenergy systems. Solar cells can also be used to feed some electrical equipment consuming a small amount of power.

Typically, this is solar radiation, but the light originated from artificial light sources can also be used to produce photocurrent [9,10]. Of course, the amount of energy that can be obtained using waste light is considerably smaller than the energy obtained from solar radiation, but it can be sufficient to power supply different kinds of sensors or controlling devices.

In many applications, waste energy, e.g., in the form of waste heat [11–18] or waste mechanical energy [19], is used to feed different sensors.

Waste light can be emitted by different artificial light sources, which are characterized with different spectral characteristics [20]. Spectral characteristics of light sources can visibly differ from spectral characteristics of solar cells sensitivity. The spectrum of daylight can change depending on the time of the day, the season, and weather conditions [21–25].

In the literature [7,9,10,26–30], many models of solar cells are described. These models describe accurately characteristics of these devices while they are irradiated by the daylight only. Optical properties of the modeled devices are characterized at given values of irradiation corresponding to the power density of solar radiation on the surface of solar cells. Meanwhile, the value of photocurrent can depend also on the spectrum of this radiation. Nonetheless, models of solar cells that are well known from the literature do not take into account the influence of spectra of the light irradiating solar cells on their properties.

In the paper, which is an extended version of the paper [31], a new model of solar cells dedicated for SPICE is presented. This model takes into account the influence of properties

of the light source that irradiates the investigated solar cells on the characteristics of these cells. The formulated model has the form of a subcircuit containing resistors and controlled current and voltage sources.

In subsequent sections of the paper, the spectral characteristics of selected light sources and the characteristics of spectral sensitivity of silicon solar cells, measured by the authors, are presented. The form of the formulated model is described in detail and the results of experimental verification of the correctness of this model while irradiating the investigated solar cells with the daylight, with a bulb, with a halogenous lamp, with a fluorescent lamp, and with LED lamps are presented. The essential influence of the applied light sources on the characteristics of solar cells is shown. It is also shown that the new model assures a good agreement between the results of computations and measurements. The possibility of a practical application of waste light to power supply electronic devices by means of solar cells is discussed.

2. Measurement of the Solar Cells Spectral Response

Figure 1 presents the setup to measure a spectral response of solar cells. This setup consists of the TLS (tunable light system) irradiating the tested solar cell (TSC) and the optical power meter (OPM) with the sensor. The TSC is connected to an ammeter.
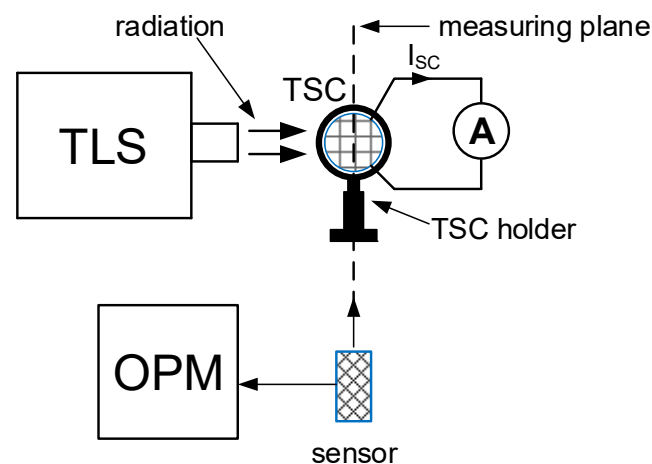
Figure 1. The setup to measure a spectral response of the tested solar cells.

The TLS (TLS-300XU [32]) produces optical radiation irradiating the tested solar cell. It includes a monochromator with the dedicated optical output and a xenon gas lamp, whose maximum value of electrical power is equal to 300 W. The spectral characteristic of the used lamp is significantly irregular. Therefore, in order to obtain a selected constant value of the optical power irradiating the surface of the solar cell, the power of the light emitted by the xenon lamp was calibrated for each used wavelength of the emitted radiation. The output optical power of the radiation produced by the TLS was fixed during calibration and it was equal to 188 μW. This power was measured using the OPHIR VEGA meter operating with the sensor PD300-UV [33].

The TLS generates the round beam of radiation of the diameter equal to about 23 mm. The solar cells tested during our investigations were cut using the fiber laser plotter Trotec Speedy 100. This plotter generates radiation of the wavelength equal to 1064 nm [34]. Next, the edges of the tested cells were polished in order to remove the products of the laser beam interaction with these cells. Finally, an ammeter measures short circuit current I_{SC} of the tested solar cells.

The spectral response of the TSC is given by the following equation [35]:

$$SR(\lambda) = I_{SC}(\lambda)/P_{OPT}(\lambda) \tag{1}$$

where P_{OPT} is the optical power of a wavelength λ. The quotient of the short current I_{SC} and the area of the tested solar cell is equal to short current density J_{SC}.

3. Measurements of Spectra of Light Sources

Spectra of the light emitted by the considered light sources are measured using the setup of the block diagram shown in Figure 2. The mentioned characteristics are measured using the compact spectroradiometer FLAME-S-XR1-ES and the software Ocean-View [36,37] operating on the personal computer (PC). The standard of spectroradiometric measurement of light sources is described in [38]. Many light sources are characterized by wide a bandwidth of the emitted light containing ultraviolet, visible light, and infrared.
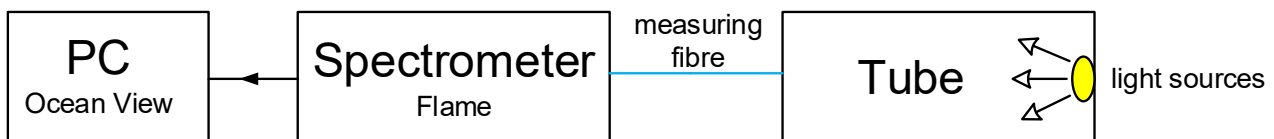
Figure 2. The setup to measure spectra characteristics of the tested light sources.

In the used spectroradiometer, there are some components such as, e.g., a diffraction grating and a CCD array used as a detector of radiation. The spectral responsivity characteristics of the mentioned components are nonlinear. Therefore, each spectroradiometer should be calibrated before starting the measurements of optical properties of this instrument [38]. In the papers [39–41], it is shown that for spectroradiometers belonging to the considered class, the calibration should be performed before starting the measurements. In this process, the radiometrically calibrated source DH-3-CAL was used. This source includes two lighting emitters: a halogen lamp and a discharge deuterium lamp, ensuring the emission of radiation in the UV-NIR range [42]. The calibration procedure was performed according to the guidelines given in [37].

The bandwidth of the used spectroradiometer contains wavelengths from 196 to 1032 nm, which contains visible light, near infrared, and near ultraviolet. This bandwidth is narrower than the bandwidth of the daylight, but it contains the whole sensitivity range of silicon solar cells [43]. In [44], the analysis of spectral characteristics of the daylight is performed in the range from 300 to 1100 nm.

During the measurements, the light sources are situated in a tube, to which the measuring fiber with the cosine corrector at the end is connected. This fiber operates in the VIS (visible light) and NIR (near infrared) spectrum regions [45]. In order to prevent optical diffusion radiation from the surroundings, the tube is inner dark.

The spectral characteristics of the tested light sources were measured using the described setup. Figure 3 shows the measured normalized spectrum of the daylight (Figure 3a) and tested light sources (Figure 3b,c). Figure 3b illustrates such characteristics for the bulb, the warm LED lamp, and the cold LED lamp, whereas Figure 3c illustrates those characteristics for the halogen lamp and the fluorescent lamp.
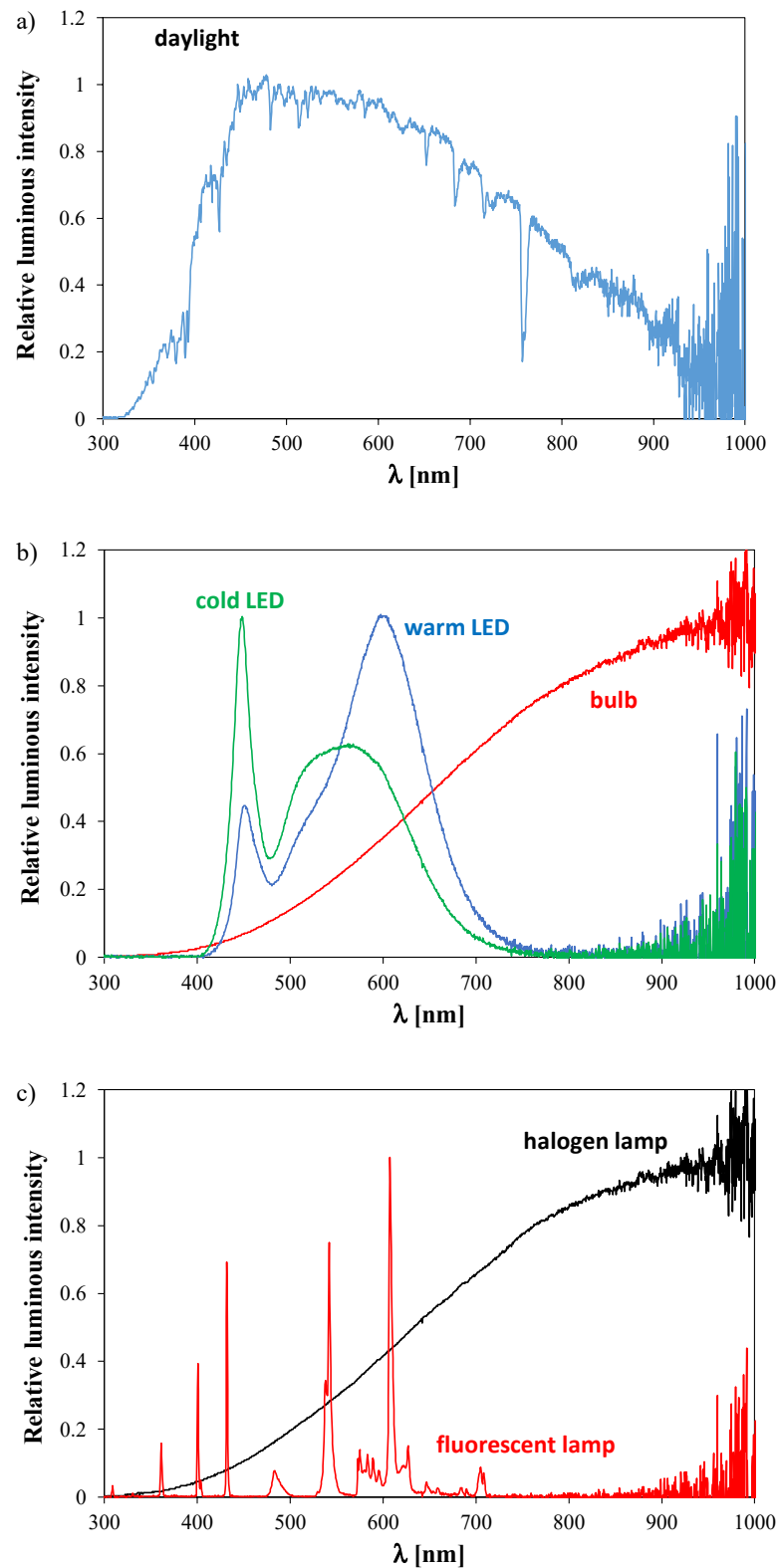
Figure 3. The measured relative spectral radiation distribution of the daylight (**a**), the bulb and the LED lamps (**b**), the halogen lamp, and the fluorescent lamp (**c**).

It can be observed in Figure 3a that radiation is emitted in the wavelength λ range wider than the wavelength range of the used instrument. According to the information given, e.g., in [46,47], the bandwidth of the daylight contains wavelengths in the range from 120 nm to 1000 μm, but 98% of solar energy is emitted in the range from 0.3 to

3 μm. For example, in the papers [48,49], the spectra of the daylight are shown. In the cited papers, it is stated that these spectra can change depending on the time, the season, and weather conditions. In Figure 3a, it is shown that in the range of visible light the maximum of the measured characteristic is observed at λ = 480 nm. Noises visible near the borders of the bandwidth are probably a result of nonideality of the used instrument. In further considerations, only the results obtained in the range from 300 to 1020 nm are used for calculations.

It is easy to notice that the shapes of spectral characteristics measured for the bulb and the halogen lamp are similar to each other. In the spectra of radiation emitted by these light sources, it is visible that the dominant part of the emitted radiation corresponds to infrared radiation. In contrast, the characteristics of the fluorescent lamp and the LED lamps are visibly different. In the characteristic of the fluorescent lamp, many local maxima can be observed. For this lamp, radiation emitted in the range of infrared radiation can be neglected. The spectra of the LED lamps contain visible light only. For the cold LED, the maximum is observed at blue light, whereas for the warm LED, the maximum is observed at yellow light. The radiation emitted in the range of ultraviolet and infrared can be neglected.

The papers [39,48] include the spectra of selected light sources. The characteristics presented in Figure 3b,c have similar shapes as the characteristics presented in the cited papers. Therefore, it can be stated that the presented in this paper characteristics are correctly measured.

All spectral radiation distributions presented in Figure 3 are measured in the range of change of the wavelength limited by the spectroradiometer used. Therefore, they can differ from the characteristics given in the literature outside the bandwidth of the used instrument.

The total power of the emitted radiation can be interpreted as the area below the considered spectral characteristics. The values of this power normalized to the value of P_{optmax} are collected in Table 1 for all the considered light sources. The computations were performed for the wavelength range from 300 to 1020 nm.

Table 1. The normalized values of the total power of radiation emitted by the tested light sources.

Light Source	Bulb	Halogen Lamp	Fluorescent Lamp	Warm LED Lamp	Cold LED Lamp	Daylight
normalized power of emitted radiation	338.4	362.9	15.5	138.9	122.3	396.1

The computed normalized power has values in the range from 15.5 for the fluorescent lamp to 362.9 for the halogen lamp. As can be observed, the considered power for the halogen lamps is only 10% lower than for the daylight. In contrast, such power for the fluorescent lamp amounts to only 4% of the value obtained for the daylight.

4. Solar Cell Model

In order to analyze properties of the investigated solar cells, the compact model of this device dedicated for SPICE was formulated. This model has the form of a subcircuit. Its network representation is given in Figure 4. This model is a modified version of the electrothermal model of the solar cell proposed in the paper [28].

The presented model belongs to the group of compact electrothermal models. In this class of models, the self-heating phenomena occurring in a semiconductor device are taken into account. Compact electrothermal models of selected semiconductor devices are described in many papers, e.g., [50–52].

In comparison to the classical models of the solar cell described, e.g., in the paper [7], the presented model takes thermal phenomena occurring in a solar cell into account. In contrast to the model described in the papers [7,9,10,26–30], the new model takes

an influence of the spectral characteristic of the light irradiating the solar cells on their characteristics into account.

The considered model consists of two parts. The first is an electrical model, whereas the other is a thermal model. The electrical model contains equations describing current-voltage characteristics of the modeled device, taking the influence of temperature into account. The thermal model makes it possible to compute the value of junction temperature T_j. This temperature is equal to the sum of ambient temperature T_a and a temperature excess caused by a phenomenon of self-heating.
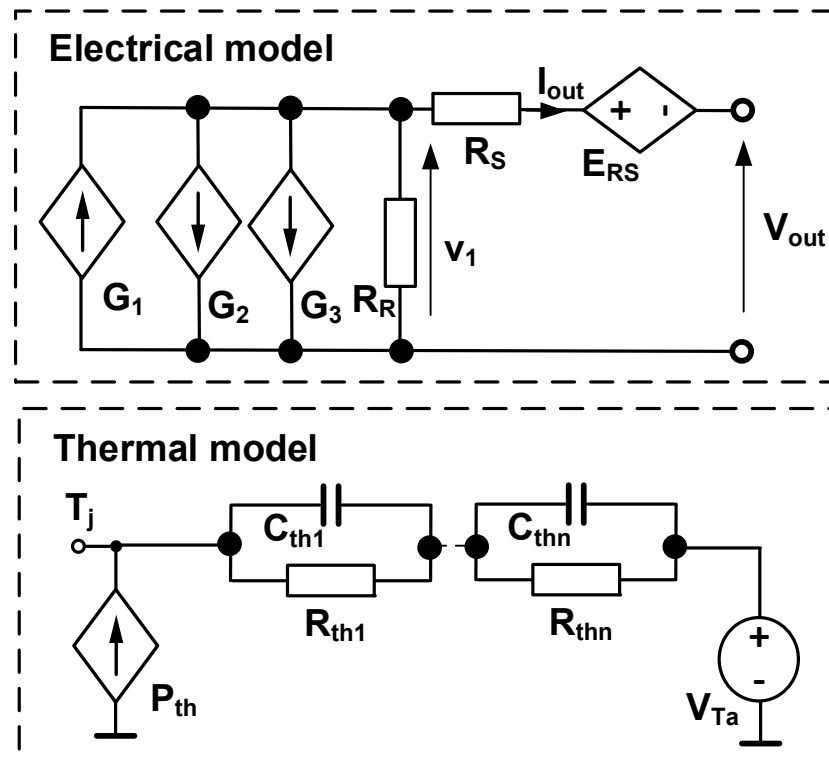
Figure 4. The network representation of the solar cell model.

The electrical model contains three controlled current sources, two resistors, and a controlled voltage source. The controlled current source G_1 models photocurrent, the controlled current source G_2 models diffusion current of the p–n junction, and the controlled current source G_3 models the generation–recombination current of this junction. Resistor R_R models leakage current, whereas resistor R_S models series resistance of the solar cell at reference temperature T_0. The dependence of series resistance on temperature is modeled by the controlled voltage source E_{RS}.

The thermal model is formulated using the classical Foster RC network [53,54]. In this network $C_{th1}, \ldots, C_{thn}$ and $R_{th1}, \ldots, R_{thn}$ are thermal capacitances and thermal resistances of the modeled device, respectively. These RC components describe the transfer of the heat generated in the solar cell to the surroundings. The controlled current source P_{th} represents the heating power equal to the sum of power of the absorbed radiation and power dissipated in the solar cell. Voltage source V_{Ta} models ambient temperature T_a.

Photocurrent is described by the following formula [55]

$$I_1 = P \cdot S \cdot \eta \cdot x \cdot a \cdot \left[1 + \alpha_T \cdot \left(T_j - T_0\right)\right] \cdot f(\varphi) \tag{2}$$

where P is irradiation of the solar cell, S is the active area of this device, η is the watt-hour efficiency of photovoltaic conversion, α_T is the temperature coefficient of the photocurrent, $f(\varphi)$ is a function of φ, where φ denotes the angle of incidence of solar beams on the surface

of the solar cell, x is the coefficient equal to 1 V^{-1}, and a is the coefficient depending on the spectrum of the light irradiating the solar cell. Parameter a is equal to 1 for the daylight.

The detailed formulae describing the other components of the presented model are given in the article [55]. The parameter values of the used model of a solar cell are as follows: $S = 0.0227$ m^2, $\eta = 0.558$, $\alpha_T = 1.8 \times 10^{-3}$ K^{-1}, $f(\varphi) = 1$, $R_S = 0.123$ Ω, $\alpha_{RS} = 3 \times 10^{-3}$ K^{-1}, $R_{sh} = 10$ kΩ, $J_{01} = 6.3 \times 10^9$ A/m^2, $n = 1.33$, $J_{02} = 5.6$ kA/m^2, $n_1 = 3.65$, $R_{th1} = 0.15$ K/W, $R_{th2} = 0.15$ K/W.

5. Results of Measurements and Computations

Measurements of the dependences of such quantities as short current and open circuit voltage of the investigated monocrystalline silicon solar cell on the wavelength of irradiating light are performed using the setup presented in Figure 1. With the use of the results of the performed measurements, a spectral response (*SR*) and external quantum efficiency of the monocrystalline silicon solar cell are computed for selected values of the wavelength. The obtained dependences are shown in Figures 5 and 6, respectively. In these figures, points denote the results of measurements, whereas lines denote the results of approximation of such results.
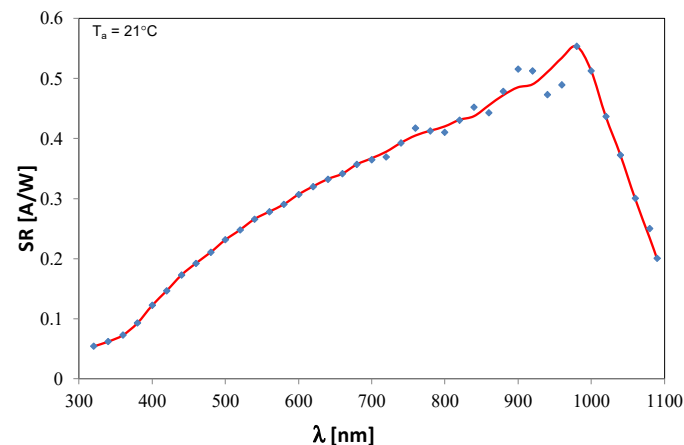
Figure 5. The measured spectral response of the tested solar cell in room temperature.
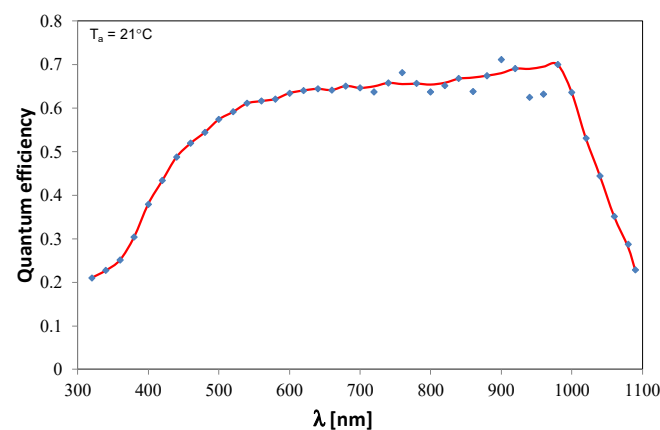
Figure 6. The measured dependence of the external quantum efficiency of the investigated solar cell on λ in room temperature.

As it can be observed in Figure 5, the highest sensitivity of the investigated solar cell is obtained at the wavelength equal to about 980 nm. For a larger wavelength, the value of the *SR* rapidly decreases, whereas in the range of a wavelength from 300 to 1000 nm, this sensitivity increases even ninefold. It should be underlined that in the region of a middle wavelength of visible light, this sensitivity is quite high.

As it is well known, the external quantum efficiency can be determined from the *SR* with the use of the following equation, presented, e.g., in [35,56]:

$$QE(\lambda) = SR(\lambda) \cdot \frac{h \cdot c}{q \cdot \lambda} \tag{3}$$

where *h* denotes Planck's constant, *c* denotes the speed of optical radiation in a vacuum, and *q* is the electron charge.

The characteristic of the external quantum efficiency of the solar cell on the wavelength (Figure 6) is almost flat for wavelengths in the range from 600 to 900 nm. The *QE* decreases even threefold for infrared and violet radiation.

Comparing the dependence $SR(\lambda)$ from Figure 5 and the spectral characteristics of the investigated light sources given in Figure 3b,c, one can observe that a high value of the power produced by the solar cell can be obtained using the light source that emits radiation in the borderland of infrared radiation and visible light.

In order to investigate the relation between the power produced in the tested solar cell irradiated from different light sources, some computations are needed. For each of the considered light sources, the values of the normalized optical power P_{nopt} from spectral characteristics of this light source are multiplied by the values of the *SR* of the tested solar cell for the same values of the wavelength. In the next step, the obtained product was integrated in the whole considered range of λ (from 320 to 1020 nm). The results of these computations (values of parameter *a*) are shown in Table 2.

Table 2. The values of the normalized power produced by the solar cell at irradiation from the tested light sources and values of parameter *a*.

Lighting Source	Bulb	Halogen Lamp	Fluorescent Lamp	Warm LED Lamp	Cold LED Lamp	Daylight
normalized optical power	153.9	162.6	3.83	41.8	33.2	126.9
parameter *a*	1.66	0.75	0.18	0.27	0.23	1

The highest values of P_{nopt} produced by the tested solar cell are obtained while it is irradiated by the halogen lamp or the bulb. At this irradiation, the value of the power is over 20% higher than at irradiation by the daylight. However, the most popular LED lamps assure a value of power produced by the tested solar cell about twice lower than the bulb. Finally, the smallest amount of power is produced at irradiation from the fluorescent lamp. In this case, the power produced by the solar cell is equal to only just 7% of this power produced at irradiation from the bulb.

The values contained in Table 2 correspond to the coefficient *a*, which occurs in the Equation (1). This parameter makes it possible to take spectral characteristics of the irradiating light source into account with respect to properties of the investigated solar cell. The coefficient *a* is estimated for each of the considered light sources on the basis of short current of the irradiated solar cell and normalized to the value of this current obtained for the daylight. Values of these parameters are in the range from 0.18 to 1.66.

In Table 3, the values of irradiation measured with the use of the radiometer HD2302.0 [57] and obtained on the surface of the investigated solar cell at its irradiation by means of different lighting sources, the luminous flux of the emitted light, and the nominal electric power are collected. For each source, different values of distances between the source housing and the sensor of the radiometer are used. The used lighting sources have a similar value of the luminous flux (about 1000 lm), but the emitting angle, wherein the light is emitted, is different for each lighting source investigated.

Table 3. The measured irradiation of the considered light sources.

Lighting Sources	Fluorescent Lamp	Halogen Lamp	Cold LED Lamp	Warm LED Lamp	Bulb
irradiation (W/m^2)	13.58	33.13	28.86	22.8	91.07
luminous flux (lm)	1100	915	1070	1050	1000
nominal electric power (W)	18	57	11.5	11.5	75

The lighting sources used during the investigations, in spite of similar values of the luminous flux, emit radiation of different values of power density. The highest irradiation equal to 91.07 W/m^2 was registered for the radiation obtained from the bulb; the lowest irradiation was equal to 13.58 W/m^2 and came from the fluorescent lamp. The value of the nominal electric power was the highest for the bulb (70 W) and the lowest for the LED lamps (11.5 W).

The tested solar cell has the dimensions 155 × 155 mm. The measurements were performed with the use of the measurement setup described in [58]. The distance between the solar cell and the lamp holder is equal to about 20 cm. The computations were performed using a DC analysis in the SPICE software.

In Figure 7, the measured and computed current–voltage characteristics of the monocrystalline solar cell lit using the considered lighting sources are shown. In turn, in Figure 8, the dependence of the power produced in the solar cell on current at its irradiation by means of different light sources is shown. The results of computations and measurements correspond to two values of ambient temperature: 300 K and 350 K.
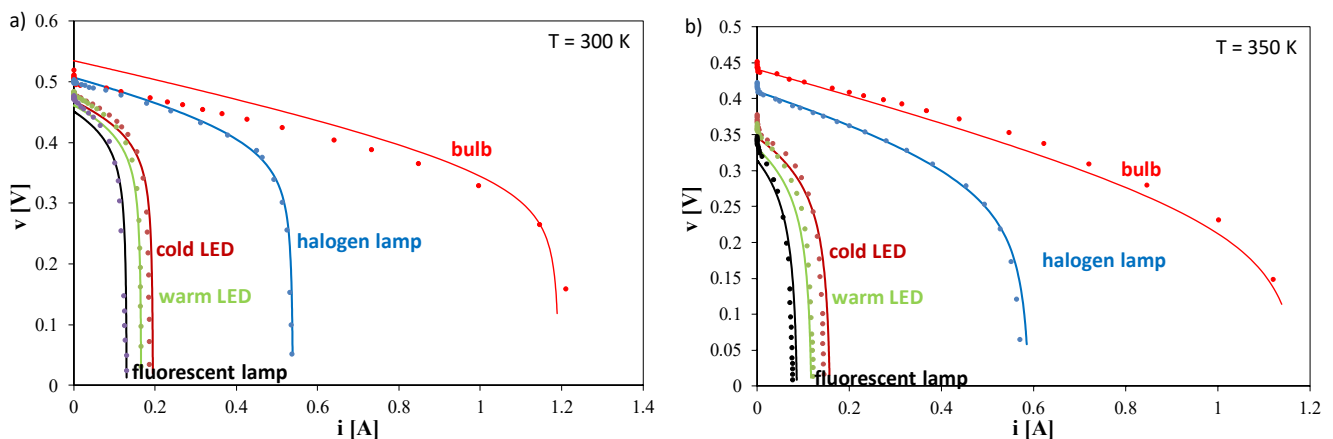
Figure 7. The measured and computed current–voltage characteristics of the monocrystalline solar cell irradiated by the considered lighting sources at temperature T = 300 K (**a**) and T = 350 K (**b**).

All the obtained v(i) dependences are decreasing functions, whereas the p(i) dependences have maxima. For different light sources irradiating the tested solar cell, different values of open circuit voltage V_{OC} and short circuit current I_{SC} are visible. Voltage V_{OC} changes even by 100 mV when the light source changes, whereas I_{SC} current changes from about 120 mV to 1.2 A.
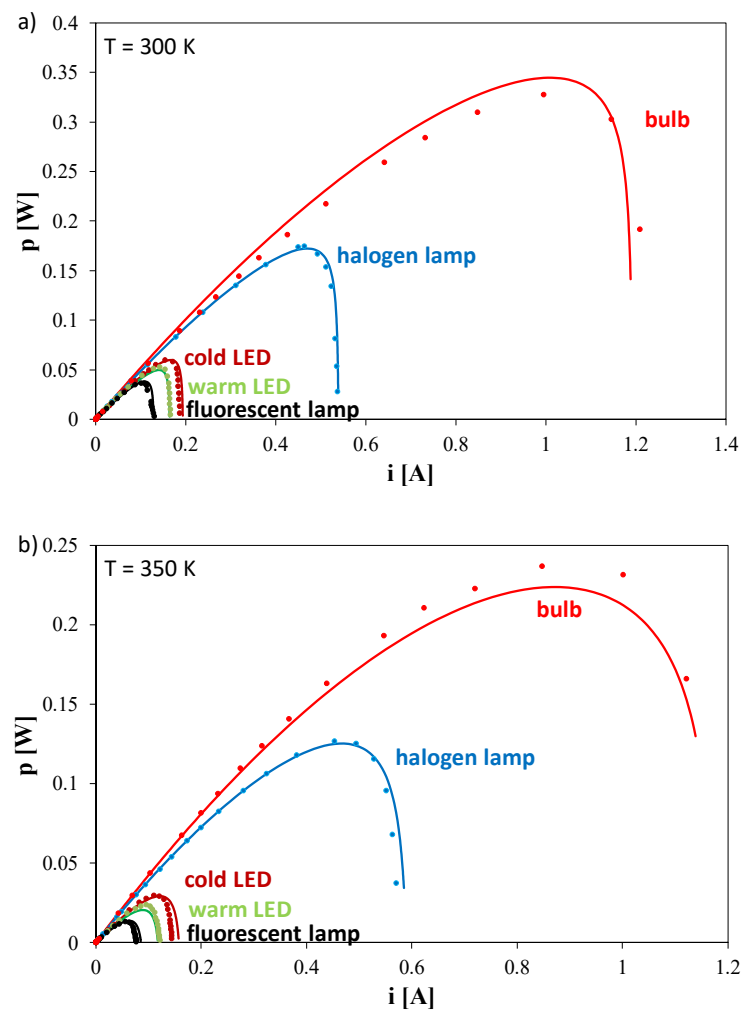
Figure 8. The measured and computed dependences of power generated in the monocrystalline solar cell on its current by irradiation of the considered lighting sources at temperature T = 300 K (**a**) and T = 350 K (**b**).

Analyzing the obtained characteristics of the monocrystalline solar cell, one can notice that the solar cell irradiated with the bulb attains the highest values of short current. In turn, while lighting the solar cell with the fluorescent lamp, one obtains the lowest values of this current. From the p(i) dependences, it is visible that the electric power generated in the solar cell while lighting it from the bulb is 10 times higher than the power produced while irradiating the solar cell from the fluorescent lamp. The difference between the power densities of radiation measured on the surface of the solar cell for these two cases is approximately seven times, which corresponds to the changes in irradiation of the solar cell.

Comparing the results of investigations obtained for different values of temperature, one can observe in Figure 7 that an increase in temperature causes a visible decrease in voltage on the tested solar cell. At a temperature increase equal to 50 K, this voltage decreases by 100 mV, which corresponds to 20% of this voltage at reference temperature T_0 = 300 K. It is also visible that short current decreases with an increase in temperature.

In turn, the maximum value of the power produced in the solar cell also decreases with an increase in temperature (Figure 8). For example, when the bulb is used to irradiate this solar cell, an increase of temperature from 300 to 350 K causes a decrease in the produced power by 30%. It is worth noticing that the value of the produced power and the value of short current are much higher for the bulb and the halogen lamp, which are characterized by the spectrum within the infrared range. In this range, the sensitivity of the solar cell is the highest.

The satisfactory agreement of the results of computations and measurements is obtained for each of the considered light sources. In order to obtain this agreement, we had to take the fact that parameter *a* depends on temperature into account.

6. Conclusions

In this paper, we presented the results of investigations illustrating the influence of the light source irradiating monocrystalline solar cells on their properties. Some measurements of a spectral response of the tested monocrystalline solar cell and the spectral characteristics of selected light sources were performed. On the basis of the results of these measurements, the values of the power produced by this solar cell operating at irradiation from the investigated light sources were estimated. The investigations were performed for artificial light sources such as a bulb, a halogen lamp, LED lamps, and a fluorescent lamp.

The new model of the solar cell is formulated. This model takes the spectral characteristics of the light sources irradiating the modeled solar cell into account. With the use of this model, the characteristics of the tested solar cell irradiated with the use of different light sources are computed. The obtained results of computations were compared to the results of measurements. The good agreement between these results proves the correctness of the proposed model.

It was shown that the use of different artificial light sources results in obtaining significantly different current–voltage characteristics and values of power produced in the irradiated solar cell. It was observed that the most profitable is the use of the halogen lamp or the bulb to irradiate the solar cell. In contrast, the lowest value of such power is obtained at irradiation from the fluorescent lamps.

The presented results of the investigations can be useful for designers of electronics networks while using solar cells to feed low power electronic equipment using waste light. If such solar cells are installed in flats or buildings, the consumption of electrical energy by electronic equipment can be reduced. Such installations can operate effectively when the daylight or artificial light of bulbs or halogen lamps is used. Such installations are not recommended for the use in the room with fluorescent lamps.

In further investigations, it would be worth analyzing the efficiency of solar cells irradiated from the source of infrared radiation.

Institutional Review Board Statement: Not applicable.

Informed Consent Statement: Not applicable.

Data Availability Statement: Data are contained within the article.

Conflicts of Interest: The authors declare no conflict of interest.

Nomenclature

a	the coefficient depending on the spectrum of the light irradiating the solar cell
c	speed of optical radiation in a vacuum
h	Planck's constant
I_{SC}	short circuit current
P	irradiation of the solar cell
P_{OPT}	optical power of incident radiation

P_{nopt}	normalized optical power
q	electron charge
QE	external quantum efficiency
S	the solar cell active area
SR	spectral response
T_a	ambient temperature
T_j	junction temperature
T_0	reference temperature
α_T	the temperature coefficient of photocurrent
φ	the angle of incidence of solar beams on the surface of the solar cell
λ	wavelength
η	watt-hour efficiency of photovoltaic conversion

References

1. Klugmann-Radziemska, E. *Fotowoltaika w Teorii i Praktyce*; Wydawnictwo BTC: Legionowo, Poland, 2010.
2. Piotrowicz, M.; Marańda, M. Sizing of Photovotaic Array for Low Feed-in Tariffs. In Proceedings of the 21th International Conference Mixed Design of Integrated Circuits and Systems (MIXDES), Lublin, Poland, 19–21 June 2014; pp. 405–408.
3. Rashid, M.H. *Power Electronic Handbook*; Elsevier: Amsterdam, The Netherlands, 2007.
4. Mulvaney, D. Solar's Green Dilemma. *IEEE Spectrum* **2014**, *51*, 30–33. [CrossRef]
5. Górecki, P. Voltage Regulators for the Laptop's Power Supply Station with Photovoltaic Modules. In Proceedings of the 22nd International Conference Mixed Design of Integrated Circuits and Systems MIXDES, Toruń, Poland, 25–27 June 2015; pp. 571–575.
6. Górecki, P.; Górecki, K.; Krac, E.; Zarębski, J. The use of photo-voltaic panels to charge mobile electronic devices. In *Proceedings of the 3rd International Congress on Energy Efficiency and Energy Related Materials (ENEFM2015), Oludeniz, Turkey, 19–23 October 2015*; Springer: Cham, Switzerland, 2017; pp. 229–234.
7. Castaner, L.; Silvestre, S. *Modelling Photovoltaic Systems Using Pspice*; John Wiley & Sons: Hoboken, NJ, USA, 2002.
8. Szul, T.; Lis, S.; Tomasik, M. Ocena efektywności energetycznej i ekonomicznej systemu grzewczego opartego na pompach ciepła typu powietrze woda współpracującego z mikroinstalacją fotowoltaiczną. *Przegląd Elektrotechniczny* **2020**, *96*, 94–97. [CrossRef]
9. Górecki, K.; Górecki, P.; Krac, E. Modelling simple photovoltaic systems with thermal phenomena taken into account. In Proceedings of the 23rd International Conference Mixed Design of Integrated Circuits and Systems MIXDES 2016, Łódź, Poland, 23–25 June 2016; pp. 276–281.
10. Górecki, K.; Dąbrowski, J.; Krac, E.; Zarębski, J. Modelling the influence of weather conditions on properties of the photovoltaic installation. In Proceedings of the 24th International Conference Mixed Design of Integrated Circuits and Systems Mixdes 2017, Bydgoszcz, Poland, 22–24 June 2017; pp. 366–371.
11. Alford, A.; Nichol, P.; Frisby, B. The Development of a Small High Speed Steam Microturbine Generator System. *IOP Conf. Ser. Mater. Sci. Eng.* **2015**, *90*, 012062. [CrossRef]
12. Suankramdee, W.; Thongtip, T.; Aphornratana, S. Development of a sliding vane expander in a micro-scale ORC system for utilizing low-grade heat. *Energy Procedia* **2017**, *138*, 817–822. [CrossRef]
13. Jouhara, H.; Khordehgah, N.; Almahmoud, S.; Delpech, B.; Chauhan, A.; Tassou, S.A. Waste Heat Recovery Technologies and Applications. *Therm. Sci. Eng. Prog.* **2018**, *6*, 268–289. [CrossRef]
14. Woolley, E.; Luo, Y.; Simeneo, A. Industrial waste heat recovery: A systematic approach. *Sustain. Energy Technol. Assess.* **2018**, *29*, 50–59. [CrossRef]
15. Sultana, A.; Alam, M.; Middya, T.R.; Mandal, D. A pyroelectric generator as a self-powered temperature sensor forsustainable thermal energy harvesting from waste heat and human bodyheat. *Appl. Energy* **2018**, *221*, 299–307. [CrossRef]
16. Su, Z.; Zhang, M.; Xu, P.; Zhao, Z.; Wang, Z.; Huang, H.; Ouyang, T. Opportunities and strategies for multigrade waste heat utilization in various industries: A recent review. *Energy Convers. Manag.* **2021**, *229*, 113769. [CrossRef]
17. Habbe, B. Thermal Energy Harvesting, Ready to Compete with Batteries? Available online: https://media.ivam.de/mikrotechnik-11/pdf/07_1430_Micropelt.pdf (accessed on 15 May 2021).
18. Miro, L.; Gasia, J.; Cabeza, L.F. Thermal energy storage (TES) for industrial waste heat (IWH) recovery: A review. *Appl. Energy* **2016**, *179*, 284–301. [CrossRef]
19. Gnutek, Z.; Poprawski, W. Niekonwencjonalne źródła energii w budowie maszyn dla budownictwa i górnictwa skalnego. *Inżynieria Masz.* **2014**, *19*, 55–62.
20. Żagan, W. *Podstawy Techniki Świetlnej*; Oficyna Wydawnicza Politechniki Warszawskiej: Warszawa, Poland, 2005.
21. Płocki, A. Funkcja sinus i nasłonecznienie. In *Matematyka w Przyrodzie i Sztuce-Matematyka, Przyroda i Sztuka w Kształceniu Powszechnym, Tom 4*, 1st ed.; Wydawnictwo Naukowe Państwowej Wyższej Szkoły Zawodowej w Nowym Sączu: Nowy Sącz, Poland, 2016; Chapter: Funkcja sinus i nasłonecznienie.
22. Matuszko, D.; Soroka, S. Spostrzeżenia dotyczące wpływu zachmurzenia na maksymalne wartości natężenia całkowitego promieniowania słonecznego. *Pr. Geogr.* **2009**, *122*, 39–48.
23. Kusznier, J. Właściwości widmowe źródeł światła typu smart LED. *Zesz. Naukowe Wydziału Elektrotechniki i Autom. Politech. Gdańskiej* **2018**, *59*, 123–126.

24. Ghazi, S.; Ip, K. The effect of weather conditions on the efficiency of PV panels in southeast of UK. *Renew. Energy* **2014**, *69*, 50–59. [CrossRef]
25. Liu, K.; Liu, W.; Gan, T.; Lai, D. Effects of Space Geometry, Season and Weather Condition on Different Components of Outdoor Thermal Radiation. In *Environmental Science and Engineering Book Series (ESE)*; Springer: Singapore, 2020.
26. Sarkar, M.N.I. Effect of various model parameter on solar photovoltaic cell simulation: A SPICE analysis. *Renewables Wind Water Sol.* **2016**, *3*, 13. [CrossRef]
27. Gadjeva, E.; Hristov, M. Behavioral Parametrized SPICE Models of Photovoltaic Modules. In Proceedings of the 20th International Conference Mixed Design of Integrated Circuits and Systems MIXDES, Gdynia, Poland, 20–22 June 2013; pp. 355–359.
28. Górecki, K.; Górecki, P.; Paduch, K. Modelling solar cells with thermal phenomena taken into account. *J. Phys. Conf. Ser.* **2014**, *494*, 012007. [CrossRef]
29. Gontean, A.; Lica, S.; Bularka, S.; Szabo, R.; Lascu, D. A Novel High Accuracy PV Cell Model Including Self Heating and Parameter Variation. *Energies* **2018**, *11*, 36. [CrossRef]
30. Krac, E.; Górecki, K. Modelling characteristics of photovoltaic panels with thermal phenomena taken into account. In *IOP Conference Series: Materials Science and Engineering, Proceedings of the 39th International Microelectronics and Packaging IMAPS Poland 2015 Conference, Gdansk, Poland, 20–23 September 2015*; IOP Publishing: Bristol, UK, 2016; Volume 104, p. 012013. [CrossRef]
31. Górecki, K.; Dąbrowski, J. Modelling properties of solar cells irradiated from different lighting sources. In Proceedings of the 2019 IEEE 13th International Conference on Compatibility, Power Electronics and Power Engineering (CPE-POWERENG), Sonderborg, Denmark, 23–25 April 2019; pp. 1–5. [CrossRef]
32. Available online: https://www.newport.com/p/TLS-300XU (accessed on 15 May 2021).
33. Available online: https://www.ophiropt.com (accessed on 15 May 2021).
34. Available online: https://www.troteclaser.com (accessed on 15 May 2021).
35. Talukdar, B.; Buragohain, S.; Kumar, S.; Umakanth, V.; Sarmah, N.; Mahapatra, S. Effect of spectral response of solar cells on the module output when individual cells are shaded. *Solar Energy* **2016**, *137*, 303–307. [CrossRef]
36. Available online: https://oceanoptics.com/product/flame-spectrometer/ (accessed on 15 May 2021).
37. Available online: https://oceanoptics.com/product/oceanview/ (accessed on 15 May 2021).
38. *The Spectroradiometric Measurement of Light Sources, Standard by Commission Internationale De L'Eclairage*; CIE 063-1984; International Commission on Illumination: Geneva, Switzerland, 1984.
39. Tabaka, P.; Jakubowski, P.; Fryc, I. Analiza wpływu czułości widmowej spektroradiometru na niedokładność pomiarów kolorymetrycznych. *Przegląd Elektrotechniczny* **2017**, *93*, 93–96. [CrossRef]
40. Zong, Y.; Brown, S.W.; Johnson, B.C.; Lykke, K.R.; Ohno, Y. Simple spectral stray light correction method for array spectrora-diometers. *Appl. Optics* **2006**, *45*, 1111–1119. [CrossRef]
41. Available online: https://research.ng-london.org.uk/scientific/spd/?page=info (accessed on 15 May 2021).
42. Deuterium-Halogen Calibration Light Source, Installation and Operation Manual, Ocean Optics. 2017. Available online: https://www.oceaninsight.com/globalassets/catalog-blocks-and-images/manuals--instruction-old-logo/radiometrically-calibrated-ls/dh-3p-installation-and-operation-manual-v1.0.pdf (accessed on 15 May 2021).
43. Gouvêa, E.C.; Sobrinho, P.M.; Souza, T.M. Spectral Response of Polycrystalline Silicon Photovoltaic Cells under Real-Use Conditions. *Energies* **2017**, *10*, 1178. [CrossRef]
44. Hernández-Andrés, J.; Romero, J.; Nieves, J.L.; Lee, R.L., Jr. Color and spectral analysis of daylight in southern Europe. *JOSA A* **2001**, *18*, 1325–1335. [CrossRef]
45. Available online: https://oceanoptics.com/product/lab-grade-patch-cords/ (accessed on 15 May 2021).
46. Kambezidis, H.D. The solar resource. In *Comprehensive Renewable Energy*; Sayigh, A., Ed.; Elsevier: Amsterdam, The Netherlands, 2012; Volume 18, pp. 27–83.
47. McVeigh, J.C.; Mech, F.I. Solar Radiation. In *Sun Power*, 2nd ed.; Elsevier: Amsterdam, The Netherlands, 1983.
48. Kusznier, J. Spectral properties of smart LED light sources. *Zeszyty Naukowe Wydziału Elektrotechniki i Automatyki PG* **2018**, *59*, 123–126. [CrossRef]
49. American Society for Testing and Materials, ASTM G173-03 Reference Spectra (2013). Available online: http://rredc.nrel.gov/solar/spectra/am1.5/ASTMG173/ASTMG173.html. (accessed on 15 May 2021).
50. Codecasa, L.; d'Alessandro, V.; Magnani, A.; Irace, A. Circuit-based electrothermal simulation of power devices by an ultrafast nonlinear MOS approach. *IEEE Trans. Power Electron.* **2016**, *31*, 5906–5916. [CrossRef]
51. Górecki, P.; Górecki, K. Modelling dynamic characteristics of the IGBT with thermal phenomena taken into account. *Microelectron. Int.* **2017**, *34*, 160–164. [CrossRef]
52. Wu, R.; Wang, H.; Pedersen, K.B.; Ma, K.; Ghimire, P.; Iannuzzo, F.; Blaabjerg, F. A Temperature-Dependent Thermal Model of IGBT Modules Suitable for Circuit-Level Simulations. *IEEE Trans. Ind. Appl.* **2016**, *52*, 3306–3314. [CrossRef]
53. Górecki, K.; Zarębski, J.; Górecki, P.; Ptak, P. Compact thermal models of semiconductor devices–a review. *Int. J. Electron. Telecommun.* **2019**, *65*, 151–158.
54. Vassighi, A.; Sachdev, M. *Thermal and Power Management of Integrated Circuits*; Springer Science + Business Media: New York, NY, USA, 2006.
55. Dąbrowski, J.; Krac, E.; Górecki, K. New model of solar cells for SPICE. In Proceedings of the 25th International Conference Mixed Design of Integrated Circuits and Systems MIXDES 2018, Gdynia, Poland, 21–23 June 2018; pp. 338–342.

56. Osterwald, C.R.; Campanelli, M.; Moriarty, T.; Emery, K.A.; Williams, R. Temperature-dependent spectral mismatch corrections. *IEEE J. Photovolt.* **2015**, *5*, 1692–1697. [CrossRef]
57. Datasheet DeltaOhm HD2302. Available online: https://www.deltaohm.com/en/wp-content/uploads/document/DeltaOHM-2302.0-Portabe-Luxmeter-Datasheet-en.pdf (accessed on 12 October 2020).
58. Górecki, K.; Krac, E. Badanie wpływu temperatury na charakterystyki fotoogniw. *Elektronika* **2014**, *9*, 95–98.